

PAPER • OPEN ACCESS

## Carbon K-edge x-ray emission spectroscopy of gas phase ethylenic molecules

To cite this article: R A Ingle *et al* 2022 *J. Phys. B: At. Mol. Opt. Phys.* **55** 044001

View the [article online](#) for updates and enhancements.

### You may also like

- [Electronic structure investigation of wide band gap semiconductors— \$\text{Mg}\_2\text{PN}\_3\$  and  \$\text{Zn}\_2\text{PN}\_3\$ : experiment and theory](#)  
Md Fahim Al Fattah, Muhammad Ruhul Amin, Mathias Mallmann *et al.*
- [Mechanism of intrinsic dipole moment induction in quantum paraelectric  \$\text{SrTiO}\_3\$](#)   
Shuhei Kawakami, Nobuo Nakajima, Masashi Nakatake *et al.*
- [Hard x-ray emission spectroscopy: a powerful tool for the characterization of magnetic semiconductors](#)  
M Rovezzi and P Glatzel







**IOP | ebooks™**

Bringing together innovative digital publishing with leading authors from the global scientific community.

Start exploring the collection—download the first chapter of every title for free.

# Carbon K-edge x-ray emission spectroscopy of gas phase ethylenic molecules

R A Ingle<sup>1,2,\*</sup> , A Banerjee<sup>3</sup>, C Bacellar<sup>2</sup>, T R Barillot<sup>2</sup>, L Longetti<sup>2</sup>, M Coreno<sup>4</sup>, M de Simone<sup>5</sup> , F Zuccaro<sup>4</sup>, L Poletto<sup>6</sup>, P Miotti<sup>6</sup>, A Röder<sup>7</sup>, A Stalow<sup>7</sup> , M S Schuurman<sup>7</sup>, M Odelius<sup>3</sup>  and M Chergui<sup>1,2,\*</sup>

<sup>1</sup> Department of Chemistry, University College London, 20 Gordon Street, London WC1H 0AJ, United Kingdom

<sup>2</sup> Laboratoire de spectroscopie ultrarapide and Lausanne Centre for Ultrafast Science (LACUS), Ecole polytechnique fédérale de Lausanne, ISIC, FSB-BSP, CH-1015 Lausanne, Switzerland

<sup>3</sup> Department of Physics, Stockholm University, AlbaNova University Center, SE-106 91 Stockholm, Sweden

<sup>4</sup> CNR—Istituto di struttura della materia (ISM), Basovizza Area Science Park, 34149 Trieste, Italy

<sup>5</sup> CNR—Istituto Officina dei Materiali (IOM), Basovizza Area Science Park, 34149 Trieste, Italy

<sup>6</sup> CNR—Istituto di Fotonica e Nanotecnologie (IFN), via Trasea 7, 35131 Padova, Italy

<sup>7</sup> Department of Chemistry, University of Ottawa, Ottawa, Ontario K1A 0R6, Canada

E-mail: [r.ingle@ucl.ac.uk](mailto:r.ingle@ucl.ac.uk) and [majed.chergui@epfl.ch](mailto:majed.chergui@epfl.ch)

Received 5 October 2021, revised 26 December 2021

Accepted for publication 24 January 2022

Published 28 February 2022



## Abstract

We report on the C K-edge x-ray absorption spectra and the resonant (RXES) and non-resonant (NXES) x-ray emission spectra of ethylene, allene and butadiene in the gas phase. The RXES and NXES show clear differences for the different molecules. Overall both types of spectra are more structured for ethylene and allene, than for butadiene. Using density functional theory—restricted open shell configuration interaction single calculations, we simulate the spectra with remarkable agreement with the experiment. We identify the spectral features as being due to transitions involving localised 1s orbitals. For allene, there are distinct spectral bands that reflect transitions predominantly from either the central or terminal carbon atoms. These results are discussed in the context of ultrafast x-ray studies aimed at detecting the passage through conical intersections in polyatomic molecules.

Keywords: x-ray emission, spectroscopy, x-ray spectroscopy, quantum chemistry

 Supplementary material for this article is available [online](#)

(Some figures may appear in colour only in the online journal)

\* Authors to whom any correspondence should be addressed.



Original content from this work may be used under the terms of the [Creative Commons Attribution 4.0 licence](#). Any further distribution of this work must maintain attribution to the author(s) and the title of the work, journal citation and DOI.

## 1. Introduction

The electronic properties of a system and its chemical bonds are ultimately determined by its valence electronic structure. Soft x-ray emission spectroscopy (XES), which involves transitions in which a vacancy in a shallow core level is filled by an electron from the outermost valence orbitals, is an ideal tool to probe the valence electronic structure with not only atomic-site specificity but also chemical specificity, especially to light atoms that are the constituents of organic molecules. Prior to the 1980s, high resolution molecular soft XES was excited using high-energy electrons in order to attain sufficient intensity [1, 2]. Measurements of pure XES spectra exclusively associated with singly excited core-hole states became possible with the availability of monochromatized x-rays from synchrotron storage rings. Tuning the energy of the incident radiation into resonance with a bound electronic transition gives rise to the so-called resonant XES (RXES), or resonant inelastic x-ray scattering (RIXS), while for excitation above the ionization threshold, non-resonant XES (NXES) occurs. The differences between RXES and NXES spectra turned out to be but one of the merits of using monochromatized synchrotron radiation as these spectral differences provide further insights into the electronic structure and the dynamics of the core and valence excited states of molecules.

As core electrons of the same elements in different chemical environments within an organic molecule (e.g. C atoms) have different binding energies, their soft XES spectra can more easily be separated [3] than is possible in x-ray absorption spectroscopy (XAS). In XAS, the contributions from atoms in non-equivalent environments can overlap each other, giving rise to spectral congestion at the edge due to core-transitions from a given inner shell. The local probe character of XES spectra has also opened new avenues to describe the bonding of molecules to surfaces [4, 5]. Indeed, for such systems it offers both elemental and chemical bonding information due to the involvement of inner, localized orbitals of well-separated energies and valence electrons. The electronic structure can thus be studied in terms of symmetry-resolved contributions to the valence band from different atomic species, and the inherent local and dipole selective properties of soft XES provide partial density of states projections on different atomic sites of a compound sample. With tuneable energy excitation one can furthermore discriminate multi-electron excitations leading to x-ray satellite lines.

Capitalizing fully on the spectral information recovered by soft XES has relied on the development of associated theoretical methods. Recent developments of multi-configurational quantum chemical methods allow for accurate simulations of x-ray spectra [6–8], and complementary methods based on density functional theory (DFT) can be applied efficiently to large systems [9]. Self-consistent field/complete active-space second-order perturbation theory/ $n$ -electron valence state perturbation theory (CASSCF/CASPT2/NEVPT2) have been employed extensively to simulate the RIXS spectra [10] and NXES. Recently the algebraic diagrammatic construction (ADC) scheme and other more accurate *ab initio* methods, like equations-of-motion coupled-cluster singles-and-doubles

have been used, with the inherent drawback of having a large computational cost [11]. CASSCF/CASPT2/NEVPT2 are restricted to limited active space which limits the energy span of the simulated spectra. All these methods are typically only applicable for small to moderate sized systems. On the other hand, DFT/restricted open shell configuration interaction single (ROCIS) has proved a blackbox and efficient way of accurately simulating the RIXS spectra and has been applied extensively to study transition metal complexes [12]. In this work, we extend this same protocol to simulate RXES spectra for organic, carbon-containing compounds.

Carbon atoms are the most important constituent of organic molecules and the role of the latter in a very wide range of natural and man-made processes need not be underscored. Carbon-containing molecules have also attracted huge interest because of their rich and diverse photophysics and photochemistry. Due to these reasons, soft XES of carbon-containing molecules have been among the most studied, both experimentally [1, 2, 13–15] and theoretically [2, 16–20]. One category of carbon-containing molecules that has attracted much interest are ethylenic systems. On the fundamental aspect, they have been studied extensively because they represent model systems for the description of one of the most fundamental unimolecular chemical events, isomerization, that drives a large class of photoinduced biological functions in nature, such as vision. The description of the electronic structure of ethylenic molecules is therefore crucial and XES is an important tool in this respect. Ever since the advent of ultrafast spectroscopy, important aspects of their dynamics have and are still being explored [21–25]. In particular, the issue of conical intersections (CIs) is a hot topic. CIs are points and lines of exact degeneracy of adiabatic electronic potential-energy surfaces in the multidimensional nuclear coordinate space of polyatomic molecules. These lines are referred to as intersection seams that form a  $3N - 8$  dimensional space, as only two coordinates lift the degeneracy of the CI, where  $N$  is equal to the number of nuclei. CIs are a theoretical concept that is now used almost universally employed to rationalise the dynamics of electronically excited states of polyatomic molecules, particularly in relation to ultrafast non-radiative relaxation [26]. The concept of CIs is therefore at the centre of the description of their ultrafast photochemistry and photophysics of polyatomic molecules. Yet, despite this central role, the actual observation of CIs has remained elusive. While the dynamics just before and just after the CI have been observed [27–31], the actual observation of passage through the CI is still lacking. The development of ultrafast element-selective core-level spectroscopies in the past two decades is opening new perspectives towards the study of molecular photophysics and photochemistry, mostly using hard x-rays [32, 33]. In the case of organic molecules, whose light atoms have their core-transitions in the soft x-ray range below 600 eV, the appearance of ultrafast soft x-ray spectroscopic methods is more recent and the field is gaining momentum [31, 34–41]. These methods offer a promising route to the detailed description of intramolecular dynamics, and in particular, CIs.

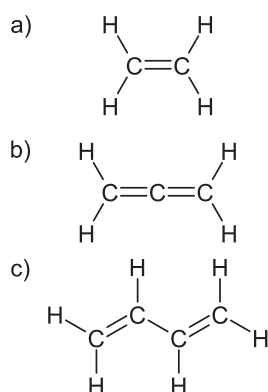


**Figure 1.** Structures of the ethylenic compounds studied in this work, hereafter referred to as (a) ethylene ( $C_2H_4$ ), (b) allene ( $C_3H_4$ ) and (c) butadiene ( $C_4H_6$ ).

Ethylenic molecules are the archetypal systems for investigation CI dynamics and in a series of recent papers [31, 42, 43], some of us presented a theoretical study of the dynamics through the CI in the case of ethylene, and translated the dynamics into XAS and x-ray photoelectron spectroscopy (XPS) observables [42, 43]. It was found that specifically at the CI, the system undergoes a sudden polarization with formation of a  $C^+ - C^-$  pair. Core-level spectroscopies are very sensitive to oxidation state changes and in reference [43], we proposed to use ultrafast XAS and XPS to detect the passage through the CI. Given that oxidation state changes are equally well detected by XES, we propose this additional avenue in the case of ethylenic systems. However, this calls for a prior investigation of the steady-state RXES and NXES spectra and the description of their electronic structure. Paradoxically, despite the interest in ethylenic systems, no such data is available on them to date. The only XES spectra of ethylenic systems in the gas phase that were reported have been obtained by electron impact (EI) excitation [16, 44]. Here we combine carbon K-edge XAS with RXES and NXES, along with density-functional theory (DFT)-based computational methods to examine the core and valence electronic structure of three ethylenic systems in the gas phase (figure 1). We show how NXES and RXES are sensitive to the chemical environment and molecular symmetry, and provide insight into the valence electronic structure of polyatomic systems. We also demonstrate how a simple theoretical protocol can accurately simulate the XES spectra for larger systems and offers an improvement over the traditionally used transition potential DFT (TP-DFT) [45] protocol of simulating XES. The new protocol makes use of the ROCIS/DFT method, and is a deviation from the standard TP-DFT method where orbitals of the non-ionized parent molecule (the moiety before photo-ionization) is used and orbital relaxation effects are grossly neglected. Our protocol with just one simple modification can capture these orbital relaxation effect, for at least the valence orbitals, to a large extent, and yet is computationally comparable to the DFT methods.

## 2. Methodology

### 2.1. Experimental methodology

Both the soft XAS and XES experiments were performed at the gasphase end station at the Elettra synchrotron radiation facility, with a synchrotron operational energy of 2.0 GeV [46]. For XAS, a monochromatized beam with approximately 100 meV output bandwidth was scanned in energy across the spectral features of interest. The resulting photoabsorption spectra were recorded by acquisition of the total ion yield using a channel electron multiplier near the interaction region. Calibration of the XAS energies was performed using  $\sim 1 \times 10^{-6}$  bar of carbon dioxide as a calibrant gas [47] in a diagnostics chamber before the interaction region. For the XES experiments, the energy calibration was performed using the scattered light peaks and the previously reported emission lines of a series of small molecules. To optimise emission signal levels in the XES experiments, the slit of the gas cell was aligned relative to the entrance slit of the spectrometer, which was mounted at magic angle ( $54.7^\circ$ ). The measured intensities have not been corrected for any self-absorption which is assumed to be minimal. All presented emission spectra are background subtracted to account for dark currents and an averaged background offset. Full details of the spectrometer have previously been reported but a brief summary will be included here [48]. For all experiments requiring detection of photon energies  $> 200$  eV, the G2400 spherical grating with a central groove density of  $2400 \text{ mm}^{-1}$  was used. The  $1340 \times 400$  pixel CCD detector was cooled to  $-40^\circ \text{C}$  for all experiments. All samples were used without further purification. They were introduced into the interaction region with a customized stainless steel gas cell. The sample cell was windowless with a transmission path length of 2 cm and a slit length of 1 cm. For the three gas phase samples (figure 1), ethylene ( $>97\%$ , Sigma Aldrich), propa-1,2-diene ( $>97\%$ , Apollo Scientific), 1,3-butadiene ( $\geq 99.6\%$ , Sigma Aldrich), the internal pressure of the gas cell was approximately 10 mbar for both emission and absorption measurements. The 1,3-butadiene sample is assumed to be exclusively in the s-trans conformation [49].

### 2.2. Computational methodology

Simulations of NXES and RXES require accurate modelling of the fluorescence decay channels from the intermediate core-hole state reached by the incident x-ray excitation. For NXES, this implies that we need to model the core-ionized state and transitions to valence-ionized states. For RXES, we need to model both the x-ray absorption to core-excited states and the transitions to valence-excited states. In addition, for accurate modelling one should consider nuclear dynamics in the processes, which have been shown to be important for ethylene and many other systems [19, 20, 50, 51]. However, in the present study dynamical effects have not been taken explicitly into account, which implies that we are neglecting vibrational envelopes and, in particular, core-hole localization.



The fact that core-hole localization is neglected also implies that the spectra we compute follow the selection rules that comply with the particular symmetry of the system, for example, in the case of centrosymmetric systems like  $C_2H_4$ , that the Laporte selection rule actually holds for the electronic transitions, and vibrational excitations are not considered.

The geometries of ethylene, allene and butadiene were optimized in the gas phase using DFT with the B3LYP functional [52, 53] and the aug-cc-pVTZ basis set [54], as implemented in the G09 quantum chemical package [55]. These optimized geometries were used to compute the NXES and RXES spectra of the respective molecules using the ORCA program package [56] version 4.2.0. Theoretical carbon K-edge spectra for XAS, NXES, and RXES were computed using DFT-ROCIS in ORCA using the same functional as for the optimization. In order to improve accuracy and cut computational cost we resort to the def2-TZVP basis set [57], which is known to satisfactorily produce the XAS spectra as shown by Neese and co-workers [12]. The computation of the XAS, RXES and NXES spectra were performed with a delocalised core hole and neglecting the effects of vibrational dynamics, including core hole localisation.

**2.2.1. RXES.** For computation of the RXES (also called RIXS), we used the RIXS module of ORCA. To speed-up the computations, the RIJCOSX protocol was also invoked and accordingly def2-TZVP/C auxiliary basis sets were used. For the SCF, a tight ( $10^{-8}$ ) convergence criterion was chosen to provide a well-converged reference wave function. DFT-ROCIS uses a set of parameters as discussed by Neese and co-workers in reference [12]. We took the three DFT-CIS-c parameters to be 0.21, 0.30 and 0.40 as prescribed by these authors [12]. The RIXS routine in ORCA requires defining three orbital spaces, i.e. a primary and secondary donor space and an acceptor space. Excitations from the secondary donor space to the acceptor space generate valence excited states and the primary donor space generates core-excited states. Thus, the energies of both valence and core excited states are generated using the DFT-ROCIS protocol. Following this, transition dipole moments between these states are computed and fed into the Kramer–Heisenberg formula to obtain the RXES profile for a selected core-excited state or for a selected energy region of incident X-rays. The acceptor space was used to adequately account for the core-excited state and also provide a large enough space to account for energy relaxation. Graphical representations of all the orbitals discussed and full tables of the computational data can be found in the supplementary information (<https://stacks.iop.org/JPB/55/044001/mmedia>) (SI), figures S1–S3 and Tables S1–S3. Based on the molecular orbitals partially depicted in figures S1–S3, the choice of primary and secondary donor and acceptor spaces for each molecule was as follows.

$C_2H_4$ : the two C 1s core-orbitals,  $1a_g$  and  $1b_{1u}$ , were chosen as a primary donor space and the rest of the doubly occupied MOs were chosen to be in the secondary donor space. The acceptor space was restricted to the lowest unoccupied molecular orbital (LUMO) ( $1b_{2g}$ ), LUMO + 1 ( $4a_g$ ) and LUMO + 2;  $C_3H_4$ : for  $C_3H_4$  we took the three C 1s core-orbitals,  $1a_1$ ,  $2a_2$

and  $1b_2$ , as primary donor space and all other occupied orbitals formed the secondary donor space. The acceptor space here was taken from LUMO ( $3e$ ) to LUMO + 9;  $C_4H_6$ : the four C 1s core-orbitals,  $1a_g$ ,  $1b_u$ ,  $2a_g$  and  $2b_u$ , were taken to be primary donor space and the remaining occupied orbitals were taken to be in the secondary donor space. Also for  $C_4H_6$  we took LUMO ( $2a_u$ ) to LUMO + 9 as the acceptor space.

Using the above mentioned protocol we compute the RXES using ORCA, which produces .rixs files containing a  $3 \times 3$  cross-section for each RIXS channel involving a specific sequence of initial, intermediate, and final states. These .rixs files were processed using our own code to generate the discrete transition energies and intensities for both core-excitations and fluorescence decay pathways into valence-excited states. Both vibrational interference and interference between core-excited states are neglected in the present work [58]. The discrete transitions are then convoluted with a symmetric pseudo-Voigt lineshape with the full width at half maximum of the Gaussian and Lorentzian components equal to 0.8 eV. For the RXES spectra, no ad hoc energy shift was applied for comparison to experiment.

**2.2.2. NXES.** NXES was also computed using the RIXS module of ORCA, but with a slightly modified protocol. The XES process involves ionization from a core orbital and decay from various occupied orbital into the core-hole, which to first approximation is independent of the energy of the incident x-ray photons. The optimization of core-hole states is generally problematic with the maximum overlap method being one of the standard protocols. Here we employ a different strategy that we believe is novel. Instead of optimizing the core ionized state, we begin with optimization of a valence ionized state, which can easily be done with standard open-shell SCF. Following this and with the corresponding quasi-restricted orbitals we employ the DFT-ROCIS protocol and the RIXS module in ORCA. The singly occupied molecular orbital (SOMO) in the doublet ground state of the cation was taken to be the acceptor space and the C 1s core orbitals were taken to be in the primary donor space. The rest of the doubly-occupied orbitals form the secondary donor space. Thus excitation from the secondary donor space to the SOMO generates various valence ionized states and the excitation from the core orbitals, i.e. primary donor space, to the SOMO generates the core ionized states, in particular, the lowest core-ionized state for each carbon atom involved in the non-resonant x-ray emission process. As depicted in figure S5, the transition dipole moments between the core-ionized and valence ionized states are computed to generate the corresponding transitions in the XES spectrum. For comparison to the experimental spectra, the discrete transitions were convoluted and an ad hoc energy shift was applied that was system dependent. For ethylene, allene and butadiene, corrections of 11.8 eV, 11.6 eV and 12.0 eV were, respectively, applied.

Here we would like to mention that if degeneracy or near-degeneracies between the highest occupied molecular orbital (HOMO) and other filled up orbitals exist, this method is prone to error, as degenerate/near-degenerate ionized states cannot be accounted for with ROCIS. The ROCIS method,

which relies on quasi-restricted orbitals, is not designed to handle such systems and gives an artificial splitting between the degenerate ionized states. We observed that by changing the first of the DFTCISc parameters it is possible to reduced this artificial splitting of energy. This change of DFTCISc values is also justifiable from the very fact that these values were optimized for transition metal L-edge XAS, whereas we deal here with purely s and p block elements and such changes are natural in order to achieve the desired accuracy. The DFT-cis parameter employed was DFTCIS-c = 0.11, 0.30, 0.40, against the standard value of 0.18, 0.30, 0.40, which is typically used for transition metal L-edge spectra.

### 3. Results and discussion

Before discussing the main experimental and computational results of RXES and NXES, we start by comparing the XAS spectra for the three ethylenic compounds of interest (figure 2). Such a comparison is key for understanding which resonances are excited in the RXES experiments and for highlighting the general differences in the electronic structure of these molecules. The XAS spectra reported here are largely consistent with previously published ones for all three molecules, with structures both in the pre-edge and near-edge regions and a largely featureless absorption at energies greater than 294 eV [59–61], decreasing in intensity as a function of energy, due to the decrease of the photoabsorption cross-section [62, 63]. The discussion here will focus on the pre-edge region, which contains contributions from several atomic transitions. The DFT-ROCIS calculations suggest that all of these arise from combinations of transitions originating from the C 1s orbitals into different unoccupied  $\pi^*$  states, consistent with previous assignments [64]. The key differences between pre-edge features of the molecules arise from the number of degenerate occupied 1s and unoccupied  $\pi^*$  orbitals.

$C_2H_2$ —for ethylene, the DFT-ROCIS calculations predict one  $1s(1b_{1u}) \rightarrow \pi^*(1b_{2g})$  transition, as is expected from the Laporte selection for centrosymmetric molecules. This is consistent with previously reported core-valence separated ADC(2) results [65]. While the experimental spectrum clearly shows more structures than would be expected for a single electronic transition, this is consistent with previously reported data and has been attributed to vibronic progressions due to dynamical effects [61].

$C_3H_4$ —for allene, there are two peaks, separated by 0.88 eV, each composed of two degenerate transitions. The electronic configurations of the three lowest energy 1s orbitals in allene, assuming  $D_{2h}$  point group, are  $(1a_1)^2(1b_2)^2(2a_1)^2$ . The  $(1b_2)^2(2a_1)^2$  levels are degenerate and 0.86 eV higher in energy than the  $(1a_1)^2$  orbital. The  $(1b_2)^2(2a_1)^2$  are localized on the two terminal carbon atoms whereas the  $(1a_1)^2$  orbital is localized on the central carbon atom. The LUMO is a pair of degenerate  $\pi^*$  orbitals of  $(3e)$  symmetry. The lower energy peak involves heavily mixed character transitions from the  $(1b_2)^2(2a_1)^2$  to the degenerate LUMO(3e) and LUMO + 1(3e), whereas the higher energy peak involves

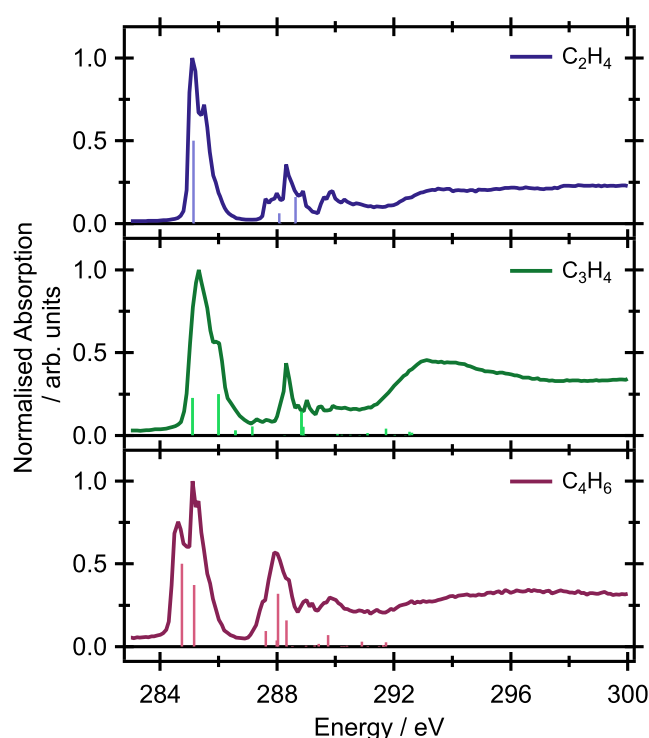


**Figure 2.** Measured XAS spectra (solid line) of (a) ethylene, (b) allene and (c) butadiene with calculated XAS transitions represented by sticks. A uniform ad hoc energy shift of 11.0, 9.95 and 10.6 eV for ethylene, allene and butadiene, respectively, was applied to the calculated transitions to match experimental data and the oscillator strengths are scaled uniformly for a visual reference.

excitation to the same final orbitals, but originating from the more tightly bound  $(1a_1)^2$ .

$C_4H_6$ —the calculated transitions for butadiene follow a similar trend but are much less mixed in character than for allene. Assuming  $C_{2h}$  symmetry, butadiene has two pairs of quasi-degenerate 1s orbitals as follows,  $(1a_g)^2(1b_u)^2$  and  $(2b_u)^2(2a_g)^2$ , with the pairs separated by 0.41 eV. Only transitions to the LUMO ( $2a_u$ ) from all four 1s orbitals are observed. The  $(1a_g)^2(1b_u)^2$  pair of orbitals are localised on the two inner carbon atoms and the  $(2b_u)^2(2a_g)^2$  pair is localized on the two terminal carbon atoms. As for allene, the lack of mixing between inner and terminal core-levels signifies the chemical shift between these sites in butadiene.

For all three molecules, this means that the energy splitting of the most intense peaks observed in the pre-edge features arises from differences in the energies of the core levels, not the final unoccupied states. In the case of allene and butadiene, this energetic separation in the core levels arises from the localization of the corresponding orbitals either on the central or terminal carbons that are in different chemical environments. Being able to differentiate between these environments from the core level energies alone has an important implication for the use of XES as a tool to study chemical dynamics, as NXES is only sensitive to energetic shifts in occupied energy levels. Particularly in the XAS spectrum of butadiene, it is clear that there are additional features present in the pre-edge structure. It is important to note that the calculations here do

not include vibronic effects and are based on single optimized geometries. Vibronic effects are known to be present in the spectrum of ethylene [19, 20, 61, 66] and, alongside nuclear quantum effects, are likely to be observed in the spectra of allene and butadiene as well [67]. Most of the analysis in this study will be based in the orbital picture, but for the prospect of following the electronic structure in transient x-ray spectroscopy it is interesting to note that in the electronic state picture, the final states in RXES consist of the ground and valence-excited states.

### 3.1. Non-resonant x-ray emission

The measured XAS spectra and accompanying calculations for the ethylenic systems studied suggest that the energy separation of the core levels should be resolvable in an XES experiment. The C K-edge XES spectrum of gaseous ethylene, recorded following EI ionization at an incident electron energy of 10 keV [44], is shown in figure 3 and is key for the validation of the photoexcitation methods used in this work. Overall, there is remarkably good agreement with the main features of the XES spectra following non-resonant x-ray excitation (at 312.0 eV). The two most intense features in both spectra are centred at 276.0 eV and 280.6 eV, with a weaker shoulder at 275.4 eV and generally broad structure appearing at higher emission energies. Notable differences occurring upon x-ray excitation are the absence or the reduced intensity, of the feature present at 278.6 eV in the EI spectrum and some differences in the low-energy shoulder of the peak at 276.0 eV. These observations most likely arise from the fact that EI also contains a contribution due to resonant excitation and indeed the peak at ca 278 eV corresponds to the main feature obtained under resonant excitation at 285.5 eV, as will be discussed later (see figure 5). In addition, differences in the selection rules governing the interaction of the molecule with either an electron or photon also play a role. The NXES of ethylene and allene bear many similarities (figures 4(a) and (b)), with two main intense peaks, a low energy shoulder on the peak around 276 eV and additional, weaker lower energy features. The spectrum of butadiene (figure 4(c)) is much more congested than the two shorter chain ethylenic systems though there appears to still be some similarities such as a relatively intense sharp feature above 280 eV and a sharp decrease in the intensity of the emission lines below 275 eV.

Before comparing the electronic structures of the three ethylenic systems, we will focus first on ethylene. For ethylene, the symmetries of the four highest energy occupied orbitals are as follows:  $(2b_{2u})^2(3a_g)^2(1b_{3g})^2(1b_{3u})^2$  (see figure S1). In the previous EI study [44], the highest energy intense emission band was assigned to emission from the HOMO  $(1b_{3u})^2$  to a hole formed in the 1s orbital following EI ionization. The series of lower energy emission lines were then attributed to transitions from the HOMO – 1 to HOMO – 4 to the same 1s energy level, with an energy progression that was approximately consistent with the valence energy level spacing reported by ultraviolet photoelectron spectroscopy [68]. The DFT-ROCIS calculations in this work (figure 4(a)) suggest that while the initial state for the four highest energy

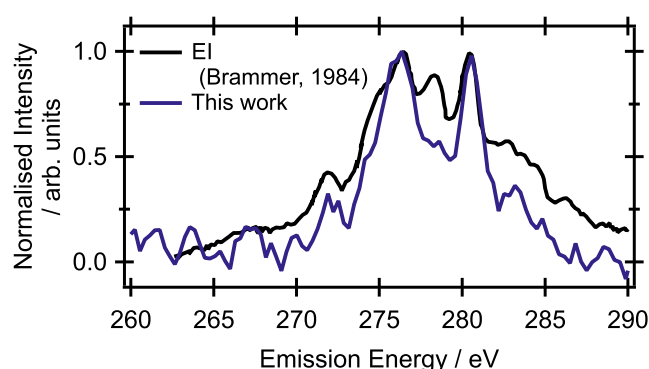


**Figure 3.** Comparison of digitized EI induced XES (Brammer, 1984) with NXES spectra upon 312.0 eV excitation of ethylene [44]. The literature data has been shifted to match the energy calibration in this work.

emission lines may be the HOMO and subsequent lower occupied orbitals, the final states may not just be the 1st orbital ( $1a_g$ ) but also the 2nd 1s orbital ( $1b_{1u}$ ). The two 1s orbitals are separated by 0.02 eV. This would mean emission from the HOMO – 2 and HOMO – 3 to the 1st 1s energy level would be forbidden by Laporte's rule and instead, the dominant contribution to the spectrum originating from these orbitals is to the 2nd 1s ( $1b_{1u}$ ) orbital. Once a suitable ad hoc energy shift (11.8 eV) is applied to the calculated emission spectrum, the overall agreement between the theoretical and experimental data is very good apart from the lower intensity of the feature at 280.6 eV. The high energy emission structure ( $>281$  eV) is likely due to satellite features, which are not accounted for in the calculations [44].

Turning now to the NXES spectrum of allene (figure 4(b)), there are two sharp features of similar intensity centred at 276.2 and 280.9 eV and a broad intensity distribution spanning from 270–285 eV. The most notable differences for allene is that the two main peaks are more pronounced relative to other spectral features and that the low energy shoulder on the peak at 276.2 is more intense than in the case of ethylene. While the general features of the experimental spectra may be similar, the calculated spectrum of allene (figure 4(b)) reveals a much more complex electronic structure. The two most intense bands both have contributions from multiple transitions, which are closely spaced in energy. Owing to the presence of degenerate occupied and unoccupied orbitals, many of the emission lines are heavily mixed in character, with contributions from multiple orbitals of the same symmetry. The highest four occupied orbitals are all of e symmetry. The lowest energy 1s MO ( $1a_1$ ) is mostly located on the central carbon, with the  $1b_2$  MO being predominantly on the terminal carbons and  $2a_1$  comprising a mixture of majority terminal but some contribution from the central carbon atom (see figure S2). The  $1b_2$  and  $2a_1$  MOs are quasi-degenerate, and 0.86 eV higher in energy than the  $1a_1$  orbital. With the exception of the contribution from the highest energy emission line which is from HOMO – 1(e)  $\rightarrow$   $1a_1(1s)$ , all of the transitions in the band at 280.9 eV are from occupied states to the 1s orbitals on the terminal carbons i.e.  $1b_2$  and  $2a_1$  MOs. For the band centred at 276.2 eV, all of the transitions are to the  $1a_1$  localised on the central carbon. As for ethylene,



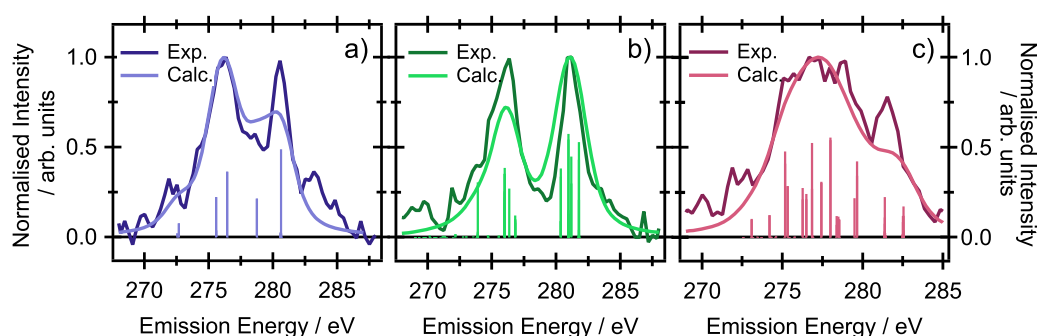


**Figure 4.** Comparison of experimental and calculated NXES spectra for (a) ethylene, (b) allene and (c) butadiene. Spectra are normalized to the most intense feature and calculated line spectra are scaled uniformly for a visual reference.

the calculations underestimate the intensity of one of the two main spectral bands.

Similar to allene, butadiene has degenerate C 1s core levels, but like ethylene, the highest energy occupied levels are non-degenerate and of different symmetries. The lowest energy pair of degenerate 1s orbitals ( $1b_u$  and  $1a_g$ ) are located on the central carbons and at 0.1 eV higher energy, there is a second degenerate pair of MOs, with nearly all of the contributing orbitals located on the terminal carbons of  $2b_u$  and  $2a_g$  symmetry (see figure S3).

Unlike the smaller hydrocarbons where the transitions are localized around specific energies, in butadiene, the overall emission spectrum is very broad. Most of the transitions are of heavily mixed character and are multiconfigurational in nature with the final states being typically a mixture of the 1st and 3rd  $1s$   $b_u$  symmetry states or the 2nd and 4th  $1a_g$  symmetry states. This makes it more complex to identify whether the emission signals are associated with the central or terminal carbons. The somewhat more resolved band at 281.5 eV involves transitions from the HOMO and HOMO – 1 to various combinations of the 1s orbitals, and the theory reproduces the experimental spectra rather well, including this peak though making it possible to disentangle some of the different types of contributions to the broad feature between 272.5 and 280.1 eV.

### 3.2. Resonant x-ray emission

In order to record resonant x-ray emission (RXES) spectra, for all three ethylenic molecules, the incident photon energies were chosen to be resonant with the pre-edge  $1s \rightarrow \pi^*$  transitions (figure 2) and the spectra are shown in figure 5. The spectra are plotted as a function of energy loss with respect to the excitation energy. Both the experimental and computed spectra are normalized to the elastic scattering peak. In figure 5, the feature at 0 eV energy loss represents the elastic scattering peak. All three molecules have an intense feature around 10 eV energy loss and a much weaker feature around 4–6 eV. For ethylene, there is only one optically bright  $1s \rightarrow \pi^*$  corresponding to a Laporte allowed  $1s(1b_{1u}) \rightarrow \pi^*(1b_{2g})$  transition in the photoexcitation window. For allene and butadiene, understanding the initial state for the RXES process is more complex. Allene has two pairs of degenerate transitions separated by 0.86 eV and butadiene has a similar structure separated by 0.40 eV. With an estimated photon bandwidth of

0.8 eV, the possibility of exciting multiple transitions cannot be excluded and will be discussed further.

The calculated energy loss spectrum predicts for ethylene two transitions with an approximate intensity ratio of 1:1.5, which corresponds to emission from the HOMO –  $1(1b_{3g}) \rightarrow$  LUMO( $1b_{2g}$ ) and HOMO –  $1(1b_{3g}) \rightarrow$  LUMO +  $1(4a_g)$  respectively (figure 5(a)). Interestingly these states corresponding to HOMO –  $1(1b_{3g}) \rightarrow$  LUMO( $1b_{2g}$ ) and HOMO –  $1(1b_{3g}) \rightarrow$  LUMO +  $1(4a_g)$  transition would be Laporte-forbidden, and hence dark in the linear absorption spectrum. The gas phase RXES spectrum presented here bears many similarities to the previously reported spectrum of ethylene in the solid state [20] though the emission band appears shifted to lower energy losses and the two involved transitions are closer in energy. For allene, the calculated RXES spectrum (figure 5(b)) reproduces the intensity distribution and shape of the experimental spectrum, albeit with the two main bands shifted to higher energy loss. The less intense feature at approx. 5 eV can be attributed to two near-degenerate mixed character transitions, which involve the same orbitals and differ by just a small difference in the mixing ratios to give rise to the 0.23 eV splitting— $(0.5)\text{HOMO} - 1(2e) \rightarrow$  LUMO( $3e$ ) +  $(0.5)\text{HOMO}(2e) \rightarrow$  LUMO +  $1(3e)$ . The higher energy loss transition involves a pair of near-degenerate transitions that are a near 50:50 mixture of HOMO –  $3(1e) \rightarrow$  LUMO( $e$ ) + HOMO –  $2(1e) \rightarrow$  LUMO +  $1(e)$  and a second pair of higher intensity transitions involving HOMO –  $4(3b_2) \rightarrow$  LUMO( $3e$ ) and HOMO –  $4(3b_2) \rightarrow$  LUMO +  $1(3e)$ . As for the NXES spectra, butadiene represents the most complex RXES case. Given the small ( $<0.5$  eV) energy separation of the two pairs of degenerate  $1s \rightarrow \pi^*$  transitions, the RXES spectra for butadiene was recorded and calculated at multiple excitation wavelengths to monitor which emission features would change upon excitation of a different electronic transition (figure 6). The most notable change in the calculated RXES spectrum on increasing the initial excitation energy is the presence of an additional transition at 7.25 eV and near doubling of the intensity of the transition at 7.49 eV. Overall, excitation via the lower energy  $1s \rightarrow \pi^*$  transition where the initial state is located primarily on the terminal carbons, results in a narrower RXES spectrum. While the signal to noise on the experimental data at the two excitation energies makes it challenging to ascertain whether the feature at 7.25 eV



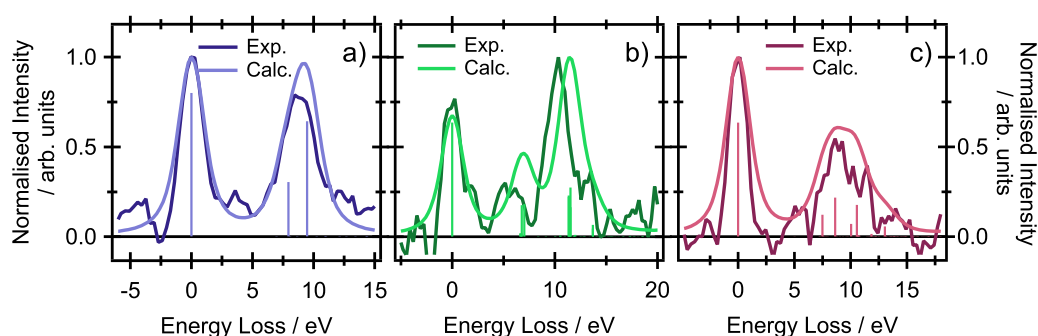


**Figure 5.** Comparison of experimental and calculated RXES spectra following excitation of the lowest energy  $1s \rightarrow \pi^*$  transition in (a) ethylene, (b) allene and (c) butadiene. Spectra are normalized to the most intense feature and calculated line spectra are scaled uniformly for a visual reference.

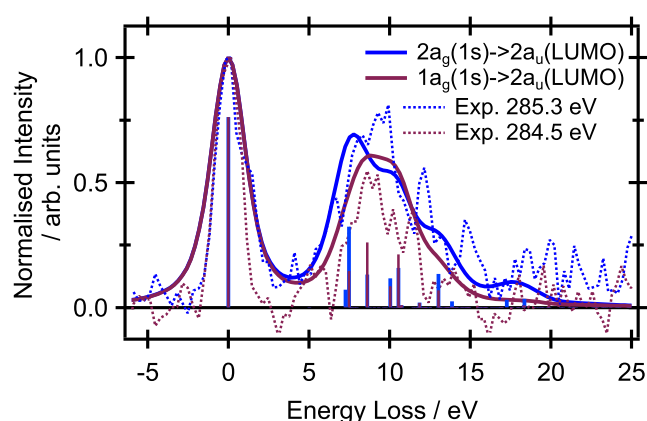


**Figure 6.** Comparison of calculated RXES spectra following resonant excitation of two different transitions for butadiene.

is indeed absent following excitation at higher energies, the trends in the intensity and spectral line widths seem to be relatively consistent with the calculated spectra. This implies that excitation at 284.5 eV results predominately in excitation of the  $(1a_g)1s \rightarrow \pi^*(2a_u)$  transition, with a negligible or no contribution from the higher lying transition. While the two RXES spectra differ in their intensity distributions, the assignments of the transitions involved are the same. The lowest energy loss transition involves the mixed character  $\text{HOMO} - 1(1a_u) \rightarrow \text{LUMO}(2a_u)$  and  $\text{HOMO}(1b_g) \rightarrow \text{LUMO} + 1(2b_g)$  and the more intense higher energy transition being from  $\text{HOMO} - 3(6b_u) \rightarrow \text{LUMO}(2a_u)$ . Both higher lying transitions are very heavily mixed, with a combination of LUMO and  $\text{LUMO} + 1$  final states. As mentioned earlier for ethylene, these transitions are Laporte-forbidden with direct excitation with visible-UV photons, but can be investigated in an RIXS measurement. The above analysis shows that to a certain extent (at least ethylene and butadiene), RXES and NXES offer the possibility to distinguish identical but non-equivalent atoms in molecules.

### 3.3. Implications for chemical dynamics

When comparing the NXES and RXES spectra for the three different molecular systems, both similarities but also

differences are observed. Ethylene can be considered the simplest case, with two identical carbon environments. The NXES spectrum still contains several transitions that reveal information on the energies of the highest occupied orbitals, with the simpler corresponding RXES spectrum consisting of two transitions that can be used to retrieve information on the energy spacing of the valence electronic states. In the case of allene, each band in the NXES spectra is associated nearly exclusively with transitions involving either just the central or the terminal carbons demonstrating the excellent sensitivity of soft XES to distinguish subtle differences in chemical environments. The systems studied are relatively large in comparison with previously studied gas phase systems using C K-edge RXES [69, 70] and it is clear that butadiene poses a challenging case with its large number of carbons and high symmetry leading to a large number of transitions, many of which are quasi-degenerate and therefore hard to resolve experimentally. However, given the excellent performance of the DFT-ROCIS methods for the calculation of spectra, it is still possible to understand many of the contribution to these spectra, despite the limitations of a single-reference method. This understanding could undoubtedly also be enhanced with further improvements in the experimental resolution, particularly for the study of more complex polyatomic systems.

Over the past few years a number of schemes, based on x-ray spectroscopies, have been proposed to observe the non-adiabatic dynamics of polyatomic molecules and in particular the dynamics through CIs [42, 43, 71–73]. In the case of ethylene, recent simulations suggested that time-resolved XAS, and to a lesser extent, time-resolved x-ray photoelectron spectroscopy, offer a uniquely sensitive probe of the passage through the CI [42, 43]. The high fluxes per pulse reached by XFELs offer the possibility to record XES spectra in a pump-probe geometry, with femtosecond duration. We propose ultrafast optical pump/soft XES probe as a third approach to probe the dynamics at the CI by detecting the changes in oxidation state. Indeed, given the clear analysis offered here of the NXES and RXES spectra and the fact that these are relatively uncongested, observing oxidation state changes should be less problematic than in the case of XAS. However, given that the dynamics through the CI can occur at extremely short time scales, e.g. in ethylene it is approx. 20 fs, the issue of intramolecular dynamics vs core-hole lifetime arises. For XES

to be a direct and unambiguous probe of the photoinduced dynamics in such experiments the lifetime of the core excited C atoms has to be significantly shorter than the CI dynamics. Core-hole lifetimes are extracted typically through lineshape analysis of high-resolution XPS data, under conditions where it can be assumed that the core-hole lifetime broadening is the dominant contribution to the observed lineshape. Some variation of this lifetime for different small molecular systems have been reported in the range of 6.1–7.4 fs [74–76] with the suggestion that the core-hole lifetime is largely unaffected by the chemical environment due to the involvement of predominantly highly localized orbitals on the carbon site [77]. When considering the accuracy of these values, it is known that even small changes in molecular geometry, such as bond extensions, can affect the extracted lifetimes [77] as can errors and uncertainties in the spectral deconvolution of the observed bands. Attosecond pulses offer a more direct probe of such lifetimes [78] though, to date, there are limited measurements of molecular systems, and for the specific case of ethylenic systems in the gas phase, none to our knowledge. Extracting a core-hole lifetime from the linewidth of the present spectra is not feasible due to the insufficient energy resolution that is limited by the spectrometer configuration. This energy bandwidth is also likely to mask any contributions from vibronic effects to the observed spectra. From comparison with other molecular systems, the ethylenic core-hole lifetime would be expected to be sub-10 fs. Given the agreement between calculations carried out on frozen Franck–Condon geometries and the experimental data presented here, it would be plausible that the molecules probed have not undergone significant structural changes on the timescale of the core-hole decay following excitation of the  $1s \rightarrow \pi^*$  transition. However, higher resolution RXES of liquid ethylene reveals vibronic contributions to the observed RXES signals, with progressively longer vibronic progressions as the initial excitation energy exceeds the energetic threshold of the first  $1s \rightarrow \pi^*$  transition [19]. The higher energy-resolution studies in the liquid phase demonstrate how the detuning modes lead to a relaxation of the selection rules and mixing of the near-degenerate gerade and ungerade core-excited states and therefore the importance of nuclear dynamics in the emission process. Still, with the lifetimes quoted above we believe that time-resolved XES is a valuable approach to probe the passage through the CI. In practical terms, for the NXES spectra recorded in this work, a signal-to-noise ratio  $> 3$  could be obtained within 3 min with a comparable photon dose ( $\sim 10^{12}$ ) to what is currently achievable at the FERMI XFEL. While a time-resolved version of the experiment would undoubtedly still be challenging with these signal levels and the introduction of a finite yield of photoexcited species, as the energy of the transitions in the NXES process is sensitive to the energetics of the C  $1s$  levels, TRXES would have the sensitivity to explore the aforementioned charge localization effects occurring at a CI. This would make it another complementary, powerful tool for exploring chemical dynamics.

Soft XES on gaseous samples will remain challenging due to the inherently unfavourable fluorescence yields for the light elements and low sample number densities. However, the development of higher repetition rate and higher flux FELs [79] will undoubtedly be an enormous benefit for such experiments, particularly for achieving sufficient flux levels that the photon bandwidth for fully exploiting resonant measurements and further suppressing satellite contributions. While this work shows that photon and electron-based excitation methods can be used for recovering similar information on the electronic structure of molecules, for future time-resolved XES measurements, photon-based excitation schemes will be the main choice. Although huge advances have been made in techniques for the temporal compression of electron bunches [80], for inefficient processes like XES, such time resolutions are not currently compatible with the magnitude of bunch charges needed or the energy flexibility for resonant experiments.

#### 4. Conclusions

This work reports for the first time C K-edge resonant and non-resonant x-ray emission spectra of three gas phase ethylenic systems, ethylene, allene and butadiene. The NXES and RXES show distinct differences in their spectral features when comparing the molecules that, with the support of high-level DFT-ROCIS calculations, we are able to associate with transition involving the localized  $1s$  orbitals. For allene, the bands can be assigned to transitions predominantly from the central or terminal carbons. There is an excellent level of agreement between the experimental and computational results and together, these results show the power of combining quantum chemical and spectroscopic approaches for understanding the electronic of molecules and the processes involved in the experimental observables. Overall, this work demonstrates the excellent sensitivity of XES to different chemical environments and its potential for future TR-XES studies.

#### Acknowledgments

This work was supported by the swiss NSF via the NCCR:MUST. MO acknowledges funding from the European Union's Horizon 2020 research and innovation programme under the Marie Skłodowska-Curie Grant Agreement No. 860553. AB and MO acknowledge funding from the Carl Tryggers Foundation (contract CTS18:285). The calculations were partially enabled by resources provided by the Swedish National Infrastructure for Computing (SNIC) at the Swedish National Supercomputer Center (NSC), The High Performance Computer Center North (HPC2N), and Chalmers Centre for Computational Science and Engineering (C3SE) partially funded by the Swedish Research Council through Grant Agreement No. 2018-05973.

## Data availability statement

The data generated and/or analysed during the current study are not publicly available for legal/ethical reasons but are available from the corresponding author on reasonable request.

## ORCID iDs

R A Ingle  <https://orcid.org/0000-0002-0566-3407>  
 M de Simone  <https://orcid.org/0000-0002-9491-0173>  
 A Stolow  <https://orcid.org/0000-0002-8447-3678>  
 M Odelius  <https://orcid.org/0000-0002-7023-2486>

## References

- [1] Tawara H, Harrison K G and De Heer F J 1973 *Physica D* **63** 351–67
- [2] Werme L O, Grennberg B, Nordgren J, Nordling C and Siegbahn K 1973 *Phys. Rev. Lett.* **30** 523–4
- [3] Nordgren J, Bray G, Cramm S, Nyholm R, Rubensson J E and Wassdahl N 1989 *Rev. Sci. Instrum.* **60** 1690–6
- [4] Nilsson A and Pettersson L G M 2004 *Surf. Sci. Rep.* **55** 49–167
- [5] Hirsch O, Kvashnina K O, Luo L, Süess M J, Glatzel P and Koziej D 2015 *Proc. Natl Acad. Sci. USA* **112** 15803–8
- [6] Coriani S and Koch H 2015 *J. Chem. Phys.* **143** 181103
- [7] Aquilante F et al 2020 *J. Chem. Phys.* **152** 214117
- [8] Wenzel J, Wornit M and Dreuw A 2014 *J. Comput. Chem.* **35** 1900–15
- [9] Fransson T, Brumboiu I E, Vidal M L, Norman P, Coriani S and Dreuw A 2021 *J. Chem. Theory Comput.* **17** 1618–37
- [10] Bokarev S I and Kühn O 2019 *Wiley Interdiscip. Rev.-Comput. Mol. Sci.* **10** e1433
- [11] Nanda K D, Vidal M L, Faber R, Coriani S and Krylov A I 2020 *Phys. Chem. Chem. Phys.* **22** 2629–41
- [12] Roemelt M, Maganas D, DeBeer S and Neese F 2013 *J. Chem. Phys.* **138** 204101
- [13] Muramatsu Y, Tomizawa K, Denlinger J D and Perera R C C 2004 *J. Electron Spectrosc. Relat. Phenom.* **137–140** 823–6
- [14] Nordgren J and Rubensson J-E 2013 *J. Electron Spectrosc. Relat. Phenom.* **188** 3–9
- [15] Guo J and Nordgren J 2000 *J. Electron Spectrosc. Relat. Phenom.* **110–111** 105–34
- [16] Manne R 1970 *J. Chem. Phys.* **52** 5733–9
- [17] Ågren H, Luo Y, Gel'mukhanov F and Jensen H J A 1996 *J. Electron Spectrosc. Relat. Phenom.* **82** 125–34
- [18] Chong D P 2020 *Can. J. Chem.* **98** 741–5
- [19] Hennies F et al 2005 *Phys. Rev. Lett.* **95** 163002
- [20] Hennies F et al 2007 *Phys. Rev. A* **76** 032505
- [21] Gloaguen E, Mestdagh J-M, Poisson L, Lepetit F, Visticot J-P, Soep B, Corioiu M, Eppink A T J B and Parker D H 2005 *J. Am. Chem. Soc.* **127** 16529–34
- [22] Mestdagh J M, Visticot J P, Elhanine M and Soep B 2000 *J. Chem. Phys.* **113** 237–48
- [23] Champenois E G, Shivaram N H, Wright T W, Yang C-S, Belkacem A and Cryan J P 2016 *J. Chem. Phys.* **144** 014303
- [24] Kosma K, Trushin S A, Fuss W and Schmid W E 2008 *J. Phys. Chem. A* **112** 7514–29
- [25] Tao H et al 2011 *J. Chem. Phys.* **134** 224306
- [26] Domcke W and Yarkony D R 2012 *Annu. Rev. Phys. Chem.* **63** 325–52
- [27] Kitney-Hayes K A, Ferro A A, Tiwari V and Jonas D M 2014 *J. Chem. Phys.* **140** 124312
- [28] Wu E C, Ge Q, Arsenault E A, Lewis N H C, Gruenke N L, Head-Gordon M J and Fleming G R 2019 *Phys. Chem. Chem. Phys.* **21** 14153–63
- [29] Yang J et al 2018 *Science* **361** 64–7
- [30] Woo K C, Kang D H and Kim S K 2017 *J. Am. Chem. Soc.* **139** 17152–8
- [31] Zinchenko K S, Ardana-Lamas F, Seidu I, Neville S P, Van Der Veen J, Lanfaloni V U, Schuurman M S and Wörner H J 2021 *Science* **371** 489–94
- [32] Milne C J, Penfold T J and Chergui M 2014 *Coord. Chem. Rev.* **277–278** 44–68
- [33] Chergui M and Collet E 2017 *Chem. Rev.* **117** 11025–65
- [34] Wernet P et al 2015 *Nature* **520** 78–81
- [35] Pertot Y et al 2017 *Science* **355** 264–7
- [36] Huse N, Kim T K, Jamula L, McCusker J K, de Groot F M F, Schoenlein R W and Schoenlein R W 2010 *J. Am. Chem. Soc.* **132** 6809–16
- [37] Huse N, Cho H, Hong K, Jamula L, De Groot F M F, Kim T K, McCusker J K and Schoenlein R W 2011 *J. Phys. Chem. Lett.* **2** 880–4
- [38] Van Kuiken B E, Cho H, Hong K, Khalil M, Schoenlein R W, Kim T K and Huse N 2016 *J. Phys. Chem. Lett.* **7** 465–70
- [39] Ekimova M, Quevedo W, Faubel M, Wernet P and Nibbering E T J 2015 *Struct. Dyn.* **2** 054301
- [40] Kleine C et al 2019 *J. Phys. Chem. Lett.* **10** 52–8
- [41] Fondell M et al 2017 *Struct. Dyn.* **4** 054902
- [42] Neville S P, Averbukh V, Patchkovskii S, Ruberti M, Yun R, Chergui M, Stolow A and Schuurman M S 2016 *Faraday Discuss.* **194** 117–45
- [43] Neville S P, Chergui M, Stolow A and Schuurman M S 2018 *Phys. Rev. Lett.* **120** 243001
- [44] Brammer R, Pettersson L, Bäckström M, Nordgren J and Nordling C 1984 *Chem. Phys. Lett.* **106** 425–7
- [45] Castillo R G, Henthorn J T, McGale J, Maganas D and DeBeer S 2020 *Angew. Chem., Int. Ed.* **59** 12965–75
- [46] Blyth R R et al 1999 *J. Electron Spectrosc. Relat. Phenom.* **101–103** 959–64
- [47] Tronc M, King G C and Read F H 1979 *J. Phys. B: At. Mol. Phys.* **12** 137–57
- [48] Poletto L et al 2014 *Rev. Sci. Instrum.* **85** 103112
- [49] Feller D and Craig N C 2009 *J. Phys. Chem. A* **113** 1601–7
- [50] Kimberg V and Rohringer N 2013 *Phys. Rev. Lett.* **110** 043901
- [51] Föhlisch A, De Groot F M F, Odelius M, Techert S and Wernet P 2014 *Phys. Rev. Lett.* **112** 129302
- [52] Becke A D 1993 *J. Chem. Phys.* **98** 5648–52
- [53] Stephens P J, Devlin F J, Chabalowski C F and Frisch M J 1994 *J. Phys. Chem.* **98** 11623–7
- [54] Kendall T H, Dunning R A Jr and Harrison R J 1992 *J. Chem. Phys.* **96** 6769
- [55] Frisch M J et al 2009 *Gaussian-09* (Wallingford CT: Gaussian Inc.)
- [56] Neese F 2012 *WIREs Comput. Mol. Sci.* **2** 73–8
- [57] Weigend F and Ahlrichs R 2005 *Phys. Chem. Chem. Phys.* **7** 3297–305
- [58] Gel'mukhanov F, Odelius M, Polyutov S P, Föhlisch A and Kimberg V 2021 *Rev. Mod. Phys.* **93** 035001
- [59] Hitchcock A P and Brion C E 1977 *J. Electron Spectrosc. Relat. Phenom.* **10** 317–30
- [60] Hitchcock A P, Johnston S, Tylliszczak T, Turci C C, Barbatti M, Rocha A B and Bielschowsky C E 2002 *J. Electron Spectrosc. Relat. Phenom.* **123** 303–14
- [61] Gadea F, Koppel H, Schirmer J, Cederbaum L, Randall K, Bradshaw A, Ma Y, Sette F and Chen C T 1991 *Phys. Rev. Lett.* **66** 883–6

- [62] Kempgens B, Köppe H M, Kivimäki A, Neeb M, Maier K, Hergenbahn U and Bradshaw A M 1997 *Phys. Rev. Lett.* **79** 35–8
- [63] Kempgens B, Köppe H M, Kivimäki A, Neeb M, Maier K, Hergenbahn U and Bradshaw A M 1999 *Surf. Sci.* **425** L376–80
- [64] Sodhi R N S and Brion C E 1985 *J. Electron Spectrosc. Relat. Phenom.* **37** 1–21
- [65] Neville S P, Averbukh V, Ruberti M, Yun R, Patchkovskii S, Chergui M, Stolow A and Schuurman M S 2016 *J. Chem. Phys.* **145** 144307
- [66] Nicolas G and Gadea F X 1999 *J. Chem. Phys.* **111** 10537–49
- [67] Schwartz C P, Uejio J S, Saykally R J and Prendergast D 2009 *J. Chem. Phys.* **130** 184109
- [68] Bieri G and Åsbrink L 1980 *J. Electron Spectrosc. Relat. Phenom.* **20** 149–67
- [69] Skytt P, Glans P, Gunnelin K, Guo J and Nordgren J 1997 *Phys. Rev. A* **55** 146–54
- [70] Magnuson M, Guo J, Sæthe C, Rubensson J-E, Nordgren J, Glans P, Yang L, Salek P and Ågren H 1999 *Phys. Rev. A* **59** 4281
- [71] Capano G, Milne C J, Chergui M, Rothlisberger U, Tavernelli I and Penfold T J 2015 *J. Phys. B: At. Mol. Opt. Phys.* **48** 214001
- [72] Kowalewski M, Bennett K, Dorfman K E and Mukamel S 2015 *Phys. Rev. Lett.* **115** 193003
- [73] Hua W, Oesterling S, Biggs J D, Zhang Y, Ando H, de Vivie-Riedle R, Fingerhut B P and Mukamel S 2016 *Struct. Dyn.* **3** 023601
- [74] Carroll T X, Hahne J, Thomas T D, Sæthre L J, Berrah N, Bozek J and Kukk E 2000 *Phys. Rev. A* **61** 042503
- [75] Forbes R, Pratt S T, De Fanis A, Milosavljević A R, Nicolas C, Bozek J D, Besley N A and Holland D M P 2020 *Phys. Rev. A* **101** 023408
- [76] Nicolas C and Miron C 2012 *J. Electron Spectrosc. Relat. Phenom.* **185** 267–72
- [77] Zahl M G, Børve K J and Sæthre L J 2012 *J. Electron Spectrosc. Relat. Phenom.* **185** 226–33
- [78] Drescher M *et al* 2002 *Nature* **419** 803–7
- [79] Gühr M 2016 *Synchrotron Radiat. News* **29** 8–12
- [80] Kim H W *et al* 2020 *Struct. Dyn.* **7** 034301